

XPS and XAS Analysis for Amorphous TiS_3 and MoS_3 Electrodes in All-solid-state Lithium Batteries

Takuya Matsuyama¹, Minako Deguchi¹, Kei Mitsuhara², Toshiaki Ohta², Takuya Mori³, Yuki Orikasa⁴, Yoshiharu Uchimoto³, Yoshiyuki Kowada⁵, Akitoshi Hayashi¹, Masahiro Tatsumisago¹

1) Graduate School of Engineering, Osaka Prefecture University, Sakai, Osaka 599-8531, Japan

2) SR Center, Ritsumeikan University, Kusatsu, Shiga 525-8577, Japan

3) Graduate School of Human and Environmental Studies, Kyoto University, Sakyo-ku, Kyoto 606-8501, Japan

4) College of Life Sciences, Ritsumeikan University, Kusatsu, 525-8577, Japan

5) Department of Natural Sciences, Hyogo University of Teacher Education, Kato, Hyogo 673-1494, Japan

Abstract

Electronic structure changes of sulfurs in amorphous TiS_3 and MoS_3 for positive electrodes of all-solid-state lithium batteries are examined by X-ray photoelectron spectroscopy (XPS) and the X-ray absorption near edge structure (XANES). The all-solid-state cell with amorphous TiS_3 electrode shows the reversible capacity of about 510 mAh g^{-1} for 10 cycles with sulfur-redox in amorphous TiS_3 during charge-discharge process. On the other hand, the cell with amorphous MoS_3 shows the 1st reversible capacity of about 720 mAh g^{-1} . The obtained capacity is based on the redox of both sulfur and molybdenum in amorphous MoS_3 . The irreversible capacity of about 50 mAh g^{-1} is observed at the 1st cycle, which is attributed to the irreversible electronic structure change of sulfur during the 1st cycle. The electronic structure of sulfur in amorphous MoS_3 after the 10th charge is similar to that after the 1st charge. Therefore, the all-solid-state cell with amorphous MoS_3 electrode shows relatively good cyclability after the 1st cycle.

This manuscript is reprinted from J. Power Sources, 313, 104 (2016), with permission from Elsevier [1].

1. Introduction

Rechargeable lithium-ion batteries with high energy density and high safety are desired as large-sized batteries for application to eco-cars and smart grids [2, 3]. However, safety is one of the most important issues to develop large-sized lithium-ion batteries because conventional lithium-ion batteries have used flammable organic liquid electrolytes. All-solid-state lithium batteries using inorganic solid electrolytes remove safety hazards associated with fire and explosion because of their advantages of leak-proof and non-flammability [4-7].

Among many kinds of lithium ion conductive solid electrolytes, sulfide-materials are known to exhibit higher ionic conductivity than oxide materials because of higher polarizability of sulfide ions [8-10]. Especially, sulfide-based solid electrolytes such as $\text{Li}_{10}\text{GeP}_2\text{S}_{12}$ crystals and $\text{Li}_2\text{S-P}_2\text{S}_5$ glass-ceramics have a high lithium-ion conductivity of almost $10^{-2} \text{ S cm}^{-1}$ at room temperature [11, 12]. This value is comparable to a conductivity of conventional organic liquid electrolytes.

To utilize the advantages of sulfide-based solid electrolytes, the development of positive electrodes is essential for all-solid-state lithium batteries. Transition metal sulfides such as TiS_2 and MoS_2 have been used as electrode materials for lithium-ion batteries using organic liquid electrolytes. In order to improve the capacities of these active materials, increasing sulfur content in the active materials is effective. Transition metal trisulfides such as TiS_3 were tested as positive electrodes in lithium-ion batteries and showed higher capacity than TiS_2 electrodes [13-15]. Amorphous transition metal trisulfides of TiS_3 and MoS_3 have high electronic conductivity and the all-solid-state cells with amorphous MS_3 (M: Ti and Mo) showed better electrochemical performance than the cells with crystalline MS_2 [16, 17]. Amorphous TiS_3 (*a-TiS*₃) exhibited a higher reversible capacity of 400 mAh g^{-1} and better cyclability than crystalline TiS_2 for 10 cycles [16]. The all-solid-state cell with amorphous MoS_3 (*a-MoS*₃) also showed the higher reversible capacity of about 670 mAh g^{-1} , compared to the cell with crystalline MoS_2 (reversible capacity: about 180 mAh g^{-1}) for 60 cycles [17]. The theoretical capacities based on transition metal-redox for crystalline TiS_2 and MoS_2 are respectively about 240 and 170 mAh g^{-1} . Amorphous TiS_3 and MoS_3 showed higher capacity than crystalline TiS_2 and MoS_2 because the redox reaction of additional sulfur would contribute to the higher capacity. However, electronic structure changes of *a-TiS*₃ and *a-MoS*₃ have not been examined for both the cells with a liquid electrolyte and a solid electrolyte. Recently, electrochemical performances of amorphous TiS_4 (*a-TiS*₄) and amorphous NbS_x ($x = 3, 4, 5$) were reported by Sakuda et al. [18-20]. The liquid-type cells using amorphous NbS_x ($x = 3, 4, 5$) showed higher discharge capacities with an increase in the sulfur content of NbS_x ; the 1st discharge capacities for amorphous NbS_3 , NbS_4 and

NbS₅ were 281, 446, and 596 mAh g⁻¹, respectively [20]. Therefore, transition metal polysulfide system is one of interesting candidates for positive electrode materials for all-solid-state lithium batteries.

Amorphous MS₃ electrode active materials are thus effective in developing all-solid-state lithium batteries with higher reversible capacity and better cyclability. In order to understand the reaction mechanisms of amorphous MS₃ electrodes in all-solid-state lithium cells, the structural changes of amorphous MS₃ during cycling tests have been examined by X-ray diffraction (XRD) measurements, Raman spectroscopy and high-resolution transmission electron microscopy (HR-TEM) [21-23]. In case of *a*-TiS₃ electrode active materials, the XRD patterns and the Raman spectra of the *a*-TiS₃ electrode after the first and tenth charge-discharge measurements were similar to those before the measurement [21, 22]. In addition, the HR-TEM images after the 10th charge-discharge tests showed no periodic lattice fringes, indicating that the *a*-TiS₃ electrode after 10 cycles did not have fine crystals with nanometer size [22]. The most part of *a*-TiS₃ electrode after charge-discharge measurements maintained amorphous structure.

In contrast, HR-TEM experiments revealed that *a*-MoS₃ before electrochemical tests was characterized by the random distribution of the nano-sized domains consisting of clusters of crystalline MoS₂ [23]. After the 1st full discharge, the lattice fringes were not observed and the electron diffraction showed halo pattern. However, the lattice fringes like MoS₂ were observed again after the 1st charge. The HR-TEM image after the 10th charge showed no lattice fringes of MoS₂. It is indicated that MoS₃ after the 10th charge was completely amorphous. However, the changes on electronic structure of sulfur and transition metal in MS₃ during cycles have not been understood yet. In order to clarify the electrochemical reaction mechanisms of amorphous MS₃, the electronic structure changes of sulfur should be examined in detail.

To examine the electronic structure changes in amorphous MS₃ during cycling in all-solid-state cells, we have used X-ray photoelectron spectroscopy (XPS) and X-ray absorption near edge structure (XANES) analysis. Previously, the electronic structure of sulfur positive electrodes after charge-discharge process was examined by S_{2p} XPS [24-28]. Diao et al. have reported that two S_{2p} peaks at 160.0 eV (Li₂S) and 161.5 eV (Li₂S₂) were observed in sulfur electrodes after the 1st discharge [24]. Helen et al. have reported that *ex-situ* S_{2p} XPS measurements were performed at various discharge and charge states during cycling; the single step transformation of sulfur to Li₂S₂ and Li₂S occurred during the charge-discharge tests in lithium-sulfur batteries [28].

In addition, XANES is a promising probe for reaction mechanism of lithium-sulfur battery [29-36]. For example, Gao et al. have reported that the effects of the electrolytes on

the electrochemical performance of lithium-sulfur batteries were examined by in-situ sulfur *K*-edge XANES [29]. Moreover, Cuisinier et al. have reported that the electronic changes of sulfur electrode in lithium-sulfur batteries during charge-discharge measurements were investigated by operando sulfur *K*-edge XANES and the mechanisms of sulfur redox chemistry on cycling were revealed [30]. As mentioned above, XPS and XANES measurements are powerful techniques to reveal the electronic structure changes of the sulfur-based electrode active materials during charge-discharge cycles.

In this study, we have firstly examined XPS and XANES to investigate electronic structure changes of sulfurs in amorphous TiS_3 and MoS_3 for all-solid-state lithium batteries with sulfide solid electrolytes during cycling. The difference of the charge-discharge mechanisms between *a*- TiS_3 and *a*- MoS_3 will be discussed.

2. Experimental

Amorphous TiS_3 (*a*- TiS_3) electrode active materials were prepared from crystalline TiS_3 (*c*- TiS_3) by the mechanical milling method [22]. Titanium metal (99.9%; Kojundo Chemical) and sulfur (99.98%; Aldrich) were used as starting materials to prepare *c*- TiS_3 . The atomic ratio of Ti to S in the starting mixture was 1/3. Titanium metal and sulfur were mixed and put into a carbon-coated quartz glass ampule and then sealed under vacuum. The glass ampule was heated at 500 °C for 8 days, and then cooled in a furnace to form *c*- TiS_3 [37]. The obtained *c*- TiS_3 was mechanically milled at ambient temperature using a planetary ball mill apparatus (Pulverisette 7; Fritsch) with zirconia pot (volume of 45 ml) and 500 zirconia balls (4 mm in diameter). The rotational speed was set to 370 rpm. The milling time was 40 h.

Amorphous MoS_3 (*a*- MoS_3) electrode active materials were prepared by mechanical milling [17]. Reagent-grade Mo metal (99.9+%; Aldrich) and sulfur (99.98%; Aldrich) were used as starting materials. The atomic ratio of Mo to S in the starting mixture was 1/3. The mixture of these materials was mechanically milled at ambient temperature using a planetary ball mill apparatus (Pulverisette 7; Fritsch) with zirconia pot (volume of 45 ml) and 500 zirconia balls (4 mm in diameter). The rotational speed was set to 370 rpm. The milling time was 80 h.

All-solid-state electrochemical cells were fabricated as follows. The 80 Li_2S ·20 P_2S_5 (mol%) solid electrolyte was prepared by the mechanical milling and then heated at 210 °C for 1 h [38]. The lithium ion conductivity of the solid electrolyte was $1.3 \times 10^{-3} \text{ S cm}^{-1}$ at 25 °C. The working electrodes of *a*- TiS_3 or *a*- MoS_3 without conductive additives and solid electrolytes were used in this study. The working electrode (10 mg) and the solid electrolyte (80 mg) were placed in polycarbonate tube (10 mm in diameter) and

pressed together under 360 MPa. A Li–In alloy was put on the solid electrolyte layer as a counter-reference electrode. A pressure of 120 MPa was then applied to the three-layered pellet. Finally, bulk-type all-solid-state cells sandwiched with two stainless-steel disks as a current collector were obtained. All processes described above were conducted in a dry Ar filled glove box. The electrochemical tests were conducted at 25 °C in an Ar filled atmosphere using a charge–discharge measuring device (BTS-2004; Nagano Co.).

The electronic structures of sulfur in *a*-TiS₃ and *a*-MoS₃ electrodes before and after charge-discharge tests were analyzed by XPS (K-Alpha; Thermo Fisher Scientific) with a Monochromatic AlK α source (1486.6 eV). The observed binding energies were calibrated with the adventitious C_{1s} peak to 284.7 eV. The samples were mounted on a sample stage in a dry Ar filled glove box and they were transferred to an analysis chamber using an Ar filled transfer vessel. XANES spectra at S *K*-edge were measured at BL-13 of the Synchrotron Radiation Center, Ritsumeikan University. The spectra were collected in total electron yield mode, wherein the sample current produced due to excitation of all electrons of different energies was measured. The sample for S *K*-edge XANES measurements were also mounted on a sample stage in a dry Ar filled glove box and they were transferred to the chamber using an Ar filled transfer vessel. We also carried out Ti and Mo *K*-edge XANES measurements at beamlines BL14B2 at SPring-8, Japan. The electrodes were sealed in laminated packets in an Ar filled glove box. The measurements were performed in a transmission mode.

3. Results and Discussion

Figure 1 shows the S_{2p} XPS spectra of *c*-TiS₃ and *a*-TiS₃ prepared in this study. The S_{2p} spectrum of *c*-TiS₃ was composed of two sets of doublet peaks (S_{2p3/2} and S_{2p1/2}). The peak energy separation (1.2 eV) in each doublet was set during peak fitting. The S_{2p} spectrum of *c*-TiS₃ showed two S_{2p3/2} peaks at 161.7 eV and 162.9 eV, respectively. The peak at 161.7 eV was characteristic of S²⁻ and the peak at 162.9 eV was characteristic of S₂²⁻ [37]. The S_{2p} spectrum of *a*-TiS₃ consisted of two S_{2p3/2} peaks at 161.3 eV and 162.5 eV, respectively. Although the peak positions were somewhat shifted to the lower binding energy side than those of *c*-TiS₃, the two peaks for *a*-TiS₃ would be assigned to S²⁻ and S₂²⁻ in the same manner for *c*-TiS₃. The fitted peak ratios of S²⁻/S₂²⁻ in *c*-TiS₃ and *a*-TiS₃ were 1/1.7 and 1/1.8, respectively.

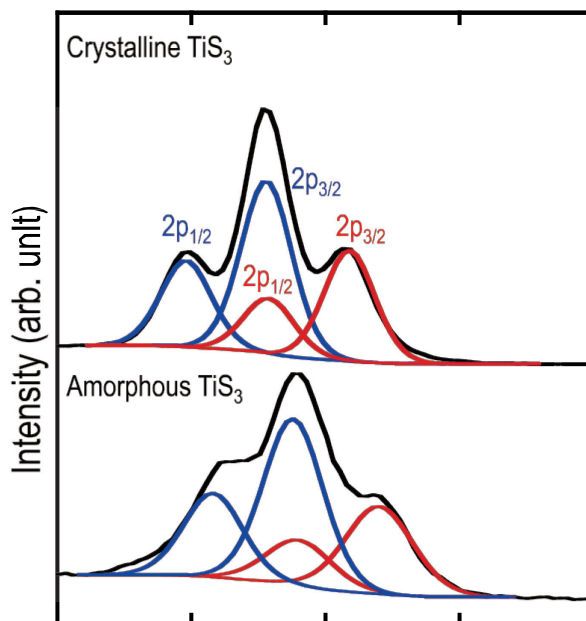


Fig. 1. S_{2p} XPS spectra of c - TiS_3 and a - TiS_3 .

Figure 2 (a) shows the 1st and 10th charge-discharge curves of all-solid-state cell with a - TiS_3 and (b) shows the S_{2p} XPS spectra of a - TiS_3 before charge-discharge, after the 1st discharge, after the 1st charge and after the 10th charge. Charge-discharge measurements of the cell with a - TiS_3 were conducted at the current density of 0.013 mA cm^{-2} (1 mA g^{-1}) at $25 \text{ }^\circ\text{C}$. In Fig. 2 (a), the right side ordinate axis represents the electrode potential vs. Li^+/Li , as calculated based on the potential difference between the Li-In and Li electrode (0.62 V). The cells using the electrode including only a - TiS_3 operated as a secondary battery. The cell using a - TiS_3 showed the reversible capacity of about 510 mAh g^{-1} for 10 cycles. This capacity corresponded to the storage of about 3 molar Li to a - TiS_3 .

The S_{2p} XPS spectrum of a - TiS_3 after the 1st discharge was shifted to the lower binding energy side. This is because Li^+ ions reacted with sulfurs in a - TiS_3 electrode active materials during discharge process. The spectrum was composed of two sets of doublet peaks. Two $S_{2p_{3/2}}$ peaks at 160.0 and 161.2 eV would be respectively attributable to S^{2-} and S_2^{2-} components interacted with both lithium and titanium. S_{2p} spectra after the 1st and 10th charge shifted to the higher binding energy side than the spectrum after the 1st discharge. The $S_{2p_{3/2}}$ peak positions of S^{2-} and S_2^{2-} after the charge were somewhat lower than those before the charge-discharge test, but the profile of the S_{2p} spectrum after the 10th charge was obviously similar to that before the test. The additional doublet peak (purple dot line) was observed slightly after the 1st and 10th charge and it would be attributable to bridging sulfurs. It is revealed that a - TiS_3 after the 10th charge mainly consisted of S^{2-} and S_2^{2-} species.

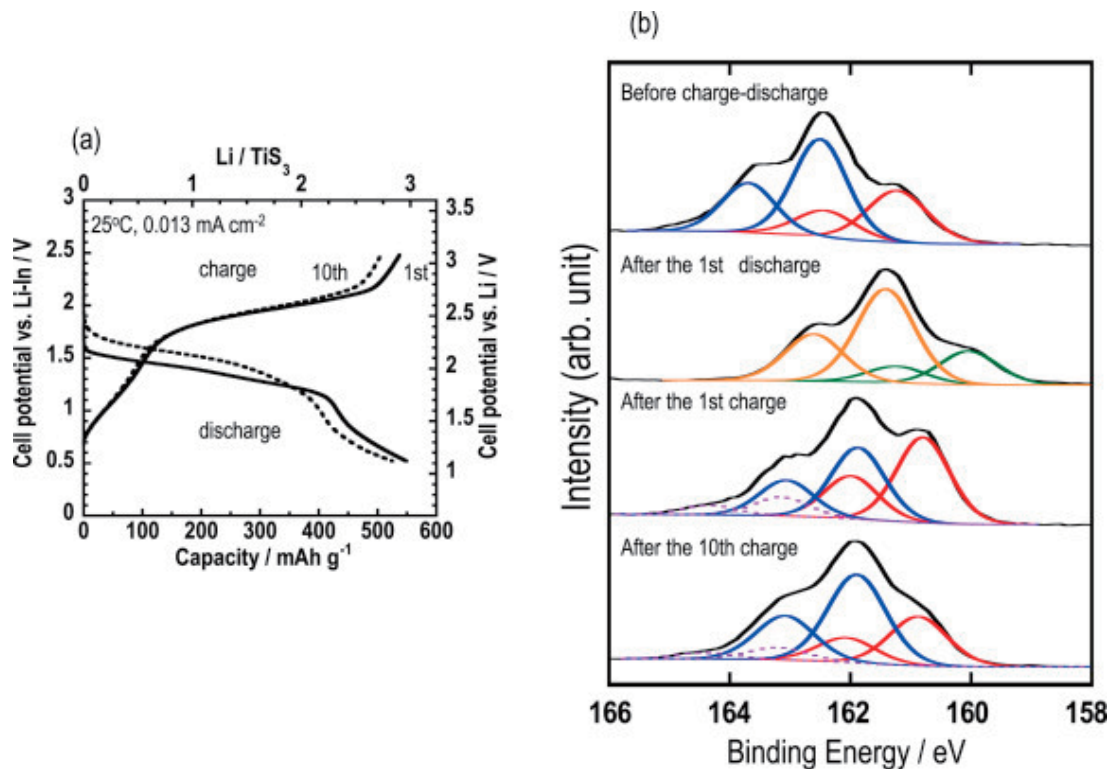


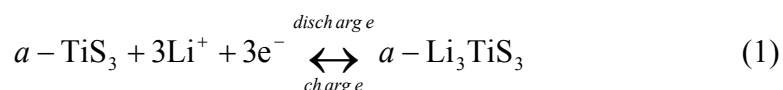
Fig. 2. (a) The 1st and 10th charge-discharge curves of the all-solid-state cell with *a*-TiS₃. (b) S_{2p} XPS spectra of *a*-TiS₃ before charge-discharge, after the 1st discharge, after the 1st charge, and after the 10th charge.

S *K*-edge XANES spectra of *a*-TiS₃ before charge-discharge, after the 1st discharge processes to 1 and 2 mol Li⁺ storage, after the 1st full discharge (3 mol Li⁺ storage), after the 1st charge and after the 10th charge are shown in Fig. 3. The peak intensity of the spectra at about 2471 eV decreased during the 1st discharge process to 2 mol Li⁺ storage. The peak position at about 2471 eV was similar to that of S₂²⁻ in *c*-TiS₃ [37], suggesting that the fraction of S₂²⁻ in *a*-TiS₃ decreased. On the other hand, after the 1st full discharge (3 mol Li⁺ storage), the spectrum profile changed significantly. Moreover, the new broad peak at about 2478 eV was observed after the 1st full discharge. This peak might be derived from sulfurs interacted with both lithium and titanium, but the detailed assignment has not been clarified yet. After the 1st and 10th charge, the profiles of the spectra were similar to that before measurements, although the peak intensity at 2471 eV became smaller. The reversible electronic structure changes of sulfur were mainly observed during charge-discharge process.

Figure 4 (a) shows Ti *K*-edge XANES spectra of *a*-TiS₃ before cycles, after the 1st discharge and after the 1st charge, and (b) shows the magnification of the XANES spectra. In addition, the spectrum of Ti metal as a reference is also shown for comparison in Fig. 4. The profiles of the spectra for *a*-TiS₃ after the 1st discharge and charge were similar to that of *a*-TiS₃ before charge-discharge. Moreover, a pre-edge peak was hardly observed in the spectra of *a*-TiS₃ before and after tests, while the spectrum of Ti metal exhibited a sharp pre-

edge peak at 4964.5 eV. It is suggested that Ti metal was not observed and the electronic structure of titanium did not change during charge-discharge. The charge-discharge curves (Fig. 2 (a)) showed 3 mol Li⁺ ions reversibly reacted with *a*-TiS₃ for 10 cycles. S_{2p} XPS spectra (Fig. 2 (b)) and S *K*-edge XANES spectra (Fig. 3) indicated that sulfur electronic structures in *a*-TiS₃ exhibited almost reversible changes during charge-discharge tests. Based on the structure analyses of *a*-TiS₃ during charge-discharge process, its reaction mechanism is proposed as follows:

equation(1)



Because the discharge plateau potential for the first 2 mol Li⁺ storage was close to the reaction potential of elemental sulfur with Li⁺, S₂²⁻ in *a*-TiS₃ reacted with 2 mol Li⁺. This agrees with the spectral changes in S *K*-edge XANES. Then, the other 1 mol Li⁺ reacted with S²⁻ to form Li₃TiS₃ after the full discharge. Because the lattice fringes were not observed in HR-TEM image after the 1st full discharge [22], Li₃TiS₃ was in amorphous state. Almost 3 mol Li⁺ ions were extracted from *a*-Li₃TiS₃ and *a*-TiS₃ was formed again after the charge process. The similar reversible reaction occurred from the 2nd to 10th cycles.

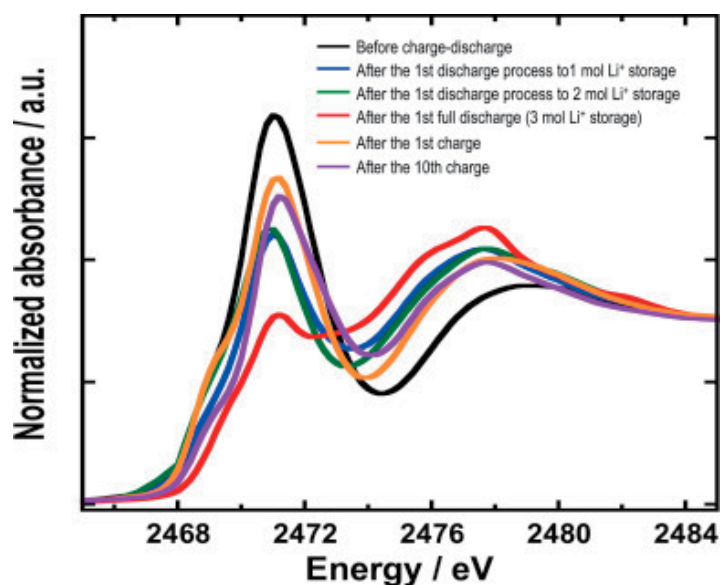


Fig. 3. S *K*-edge XANES spectra of *a*-TiS₃ before charge-discharge, after the 1st discharge processes to 1 and 2 mol Li⁺ storage, after the 1st full discharge (3 mol Li⁺ storage), after the 1st charge and after the 10th charge.

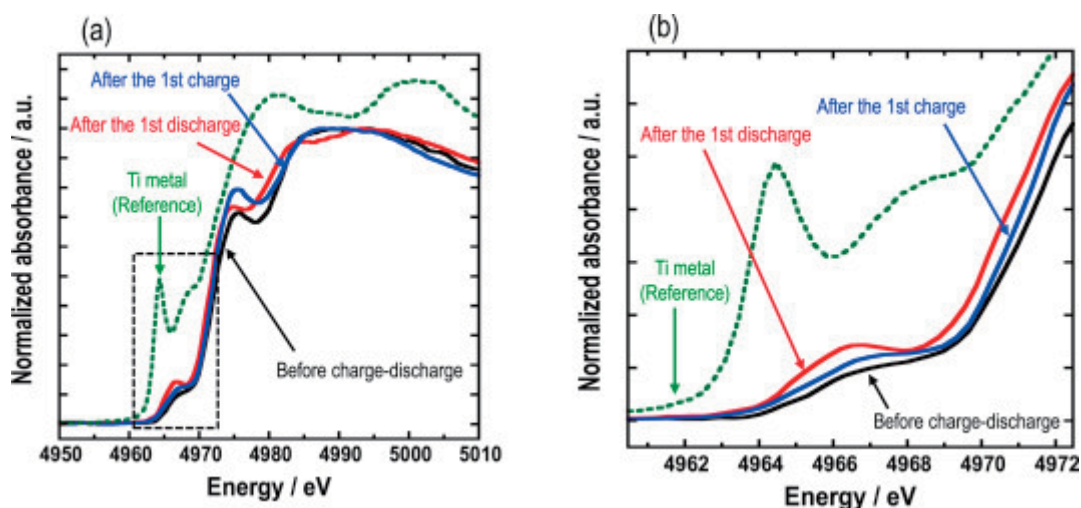


Fig. 4. (a) Ti *K*-edge XANES spectra of *a*-TiS₃ before, after the 1st discharge and after the 1st charge, and (b) the magnification of the XANES spectra. The spectrum of Ti metal as a reference is also shown for comparison.

3.2. Structural analyses of *a*-MoS₃ electrode

Figure 5 (a) shows the 1st and 10th charge-discharge curves of all-solid-state cell with *a*-MoS₃ and (b) shows the S_{2p} XPS spectra of *a*-MoS₃ before cycles, after the 1st discharge, after the 1st charge and after the 10th charge. Charge-discharge measurements of the cell with *a*-MoS₃ were conducted at the current density of 0.013 mA cm⁻² (1 mA g⁻¹) at 25 °C. In Fig. 5 (a), the right side ordinate axis represents the electrode potential vs. Li⁺/Li, as calculated based on the potential difference between the Li-In and Li electrode (0.62 V). The cells using the electrode including only *a*-MoS₃ operated as a secondary battery. The 1st discharge and charge capacities of the cell with *a*-MoS₃ were about 760 and 720 mAh g⁻¹, respectively. The irreversible capacity was observed at the 1st cycle. After the 10th cycle, the cell using *a*-MoS₃ showed the reversible capacity of about 670 mAh g⁻¹.

The S_{2p} XPS spectrum of *a*-MoS₃ before charge-discharge showed the two S_{2p_{3/2}} peaks at 162.2 and 163.4 eV. The peak at 162.2 eV was almost the same as the peak at 162.5 eV attributable to S²⁻ in crystalline MoS₂ [39]. In our previous article [23], the peak at 163.4 eV was assigned to S₂²⁻. We have measured S_{2p} spectra for reference samples of Na₂S₄ and elemental sulfur (S₈). Crystalline Na₂S₄ has two sulfur species of terminal non-bridging S⁻ and bridging sulfur S⁰ in S—S bond. The peak of *a*-MoS₃ at 163.4 eV exhibited between the S_{2p_{3/2}} peak at 162.8 eV of bridging sulfur in the S—S bond combined with S⁻ in Na₂S₄ and the S_{2p_{3/2}} peak at 164.0 eV of bridging sulfur with long chain in S₈. We have thus assigned the S_{2p_{3/2}} peak of *a*-MoS₃ at 163.4 eV to bridging sulfur with longer chain than S—S (S₂) having partial negative charge. The S_{2p_{3/2}} peak of *a*-MoS₃ at 163.4 eV is expressed as S^{δ-} in the following discussion. The fitted S²⁻/S^{δ-} peak ratio was 2.2/1. As a result, *a*-

MoS₃ consisted of S²⁻ in MoS₂ nano-clusters detected by HR-TEM [17] and S^{δ-}.

The S_{2p} XPS spectrum of *a*-MoS₃ after the 1st discharge was shifted to the lower binding energy side. This is because Li⁺ ions reacted with sulfur in *a*-MoS₃ electrode active materials during discharge process. Two S_{2p_{3/2}} peaks at 159.9 and 161.4 eV are possibly assigned to S^{δ-} and S²⁻ interacted with both lithium and molybdenum. The peak positions of two S_{2p_{3/2}} peaks after the 1st and 10th charge were different from those before charge-discharge and almost the same as those after the 1st discharge.

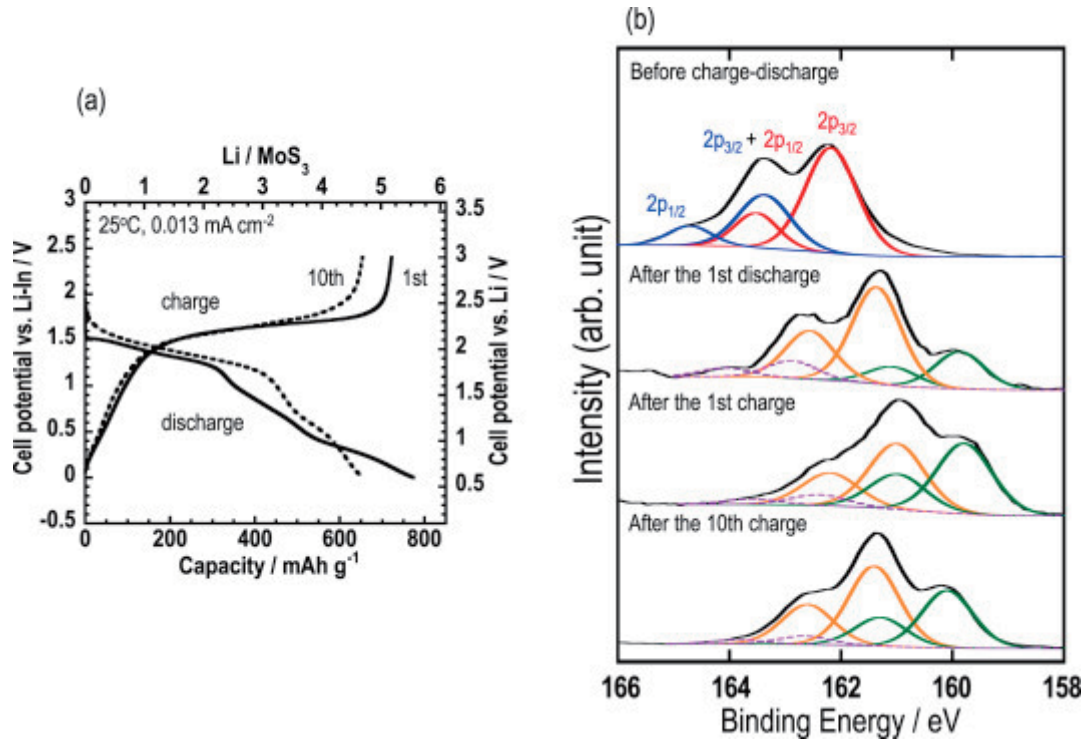


Fig. 5. (a) The 1st and 10th charge-discharge curves of all-solid-state cell with *a*-MoS₃ and (b) the S_{2p} XPS spectra of *a*-MoS₃ before charge-discharge, after the 1st discharge, after the 1st charge and after the 10th charge.

Figure 6 shows the S *K*-edge XANES spectra of *a*-MoS₃ before charge-discharge, after the 1st discharge, after the 1st charge and after the 10th charge. The peak sharpness of *a*-MoS₃ before charge-discharge at about 2471 eV was different from that of *a*-TiS₃. It is suggested that the electronic structure of sulfur in *a*-MoS₃ was not the same as that in *a*-TiS₃. After the 1st discharge, the profile of S *K*-edge XANES spectrum changed drastically. It is suggested that the electronic structures of sulfur changed by lithiation process. The profiles of the S *K*-edge XANES spectra of *a*-MoS₃ after the 1st and 10th charge were not the same as that of *a*-MoS₃ itself. Consequently, the electronic structures of sulfur did not change reversibly. However, the profiles of the spectra after the 1st and 10th charge were similar to those after the 1st discharge. Moreover, the peak at about 2473 eV was observed in the spectra except for *a*-MoS₃ before test. This peak is attributable to S²⁻ in Li₂S [29-36]. The new broad

peak at about 2476 eV was observed after the 1st discharge, 1st charge and 10th charge. This peak might be derived from sulfurs interacted with both lithium and molybdenum, but detailed assignment has not been clarified yet.

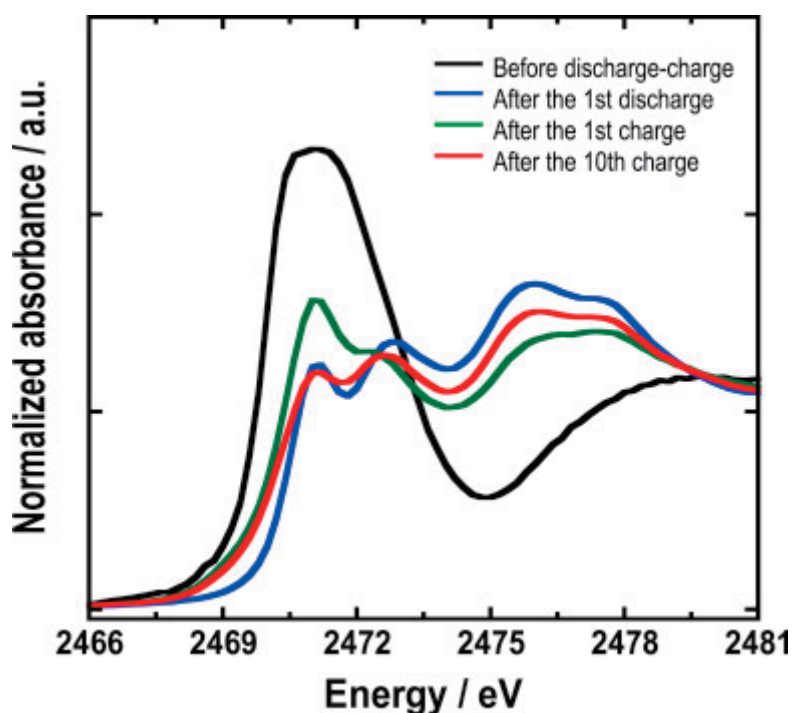


Fig. 6. S K-edge XANES spectra of *a*-MoS₃ before charge-discharge, after the 1st discharge, after the 1st charge and after the 10th charge.

Figure 7 (a) shows Mo *K*-edge XANES spectra of *a*-MoS₃ before cycles, after the 1st discharge and after the 1st charge and (b) shows the magnification of the XANES spectra. In addition, the spectrum of Mo metal is also shown for comparison in Fig. 7. Mo *K*-edge XANES spectra after discharge shifted to the lower energy side, which indicates the reduction of molybdenum. However, the profile of the spectrum for *a*-MoS₃ after the 1st discharge did not coincide with that of Mo metal as a reference, suggesting that molybdenum was not metallic state. After the 1st charge, the spectrum was similar to that before tests. The reversible change of electronic structure in molybdenum was observed.

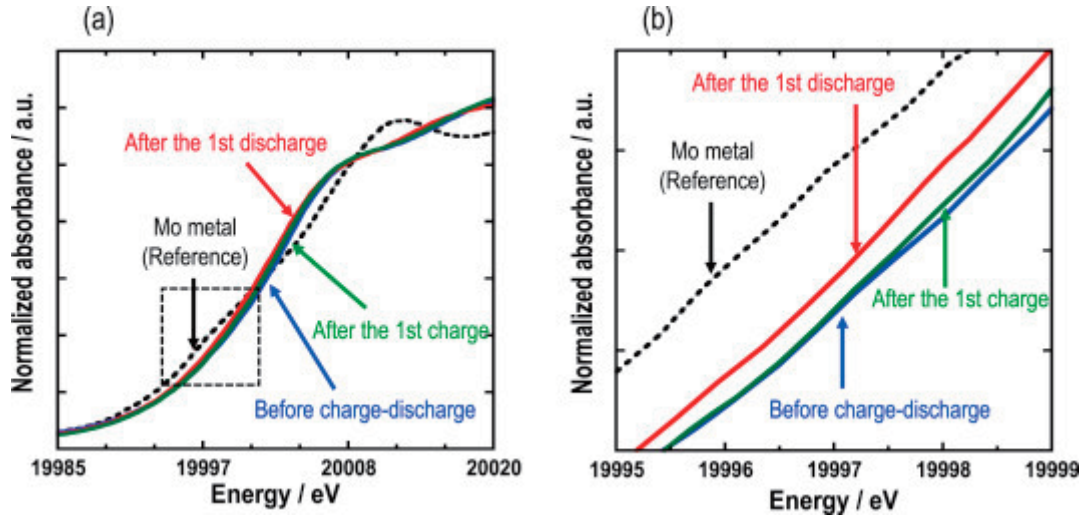
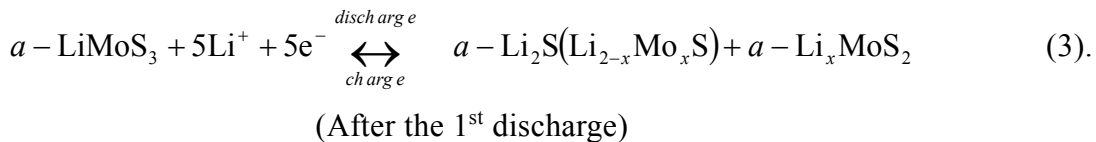
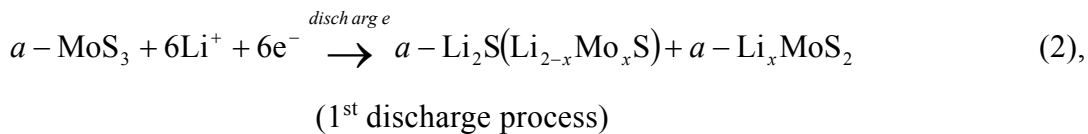


Fig. 7. (a) Mo *K*-edge XANES spectra of *a*-MoS₃ before, after the 1st discharge and after the 1st charge, and (b) the magnification of the XANES spectra. The spectrum of Mo metal is also shown for comparison.

On the basis of the results of charge-discharge curves (Fig. 5 (a)), *a*-MoS₃ reacted with about 6 mol Li⁺ ions at the 1st discharging process, while 5 mol Li⁺ ions were extracted at the 1st charging process. The reversible reaction with about 5 mol Li⁺ ions occurred during 10 cycles. From the result of Mo *K*-edge XANES (Fig. 7), the electronic structures of molybdenum changed reversibly during electrochemical tests. From the results of S_{2p}XPS (Fig. 5 (b)) and S *K*-edge XANES (Fig. 6), the irreversible electronic structure changes of sulfur were observed during the 1st charge-discharge process. This is a possible reason for the 1st irreversible capacity of the cell using *a*-MoS₃. The electronic structure of sulfur after the 10th charge was similar to that after the 1st charge. Based on the structure analyses of *a*-MoS₃ during charge-discharge process, its reaction mechanism is proposed as follows:



The discharge plateau potential of the cell using *a*-MoS₃ at about 2.0 V vs. Li as shown in Fig. 5 (a) was higher than that of the cell using crystalline MoS₂ at about 1.0 V vs. Li [17]. This suggests that S^{δ-} ions in *a*-MoS₃ would firstly react with Li⁺ ions during discharge process from 2.0 to 1.6 V vs. Li. The cell using *a*-MoS₃ operated near the electrochemical potential of sulfur. After reacted with 2 mol Li⁺ ions at about 2.0 V, Li₂S and/or its solid

solutions ($\text{Li}_{2-x}\text{Mo}_x\text{S}_2$), where a small amount of Mo is substituted for Li, were formed. Because S^{2-} in crystalline MoS_2 reacted with Li^+ ions below 1.6 V vs. Li, 4 mol Li^+ ions reacted with S^{2-} in $a\text{-MoS}_3$ to form Li_xMoS_2 at the 1st lithiation process below 1.6 vs. Li. HR-TEM analyses indicated these discharge products were amorphous state [23]. After the 1st charge, 5 mol Li^+ ions were extracted from the discharge products and thus amorphous LiMoS_3 would be formed. As shown in S_{2p} XPS (Fig. 5)(b) results, the S_{2p} XPS spectrum was shifted to the lower binding energy side after the 1st full discharge, suggesting that S^{2-} and $\text{S}^{\delta-}$ species interacted with both lithium and molybdenum. The S K -edge XANES spectrum (Fig. 6) and Mo K -edge XANES spectrum (Fig. 7) changed during the 1st discharge process. These results agree with the reaction mechanism of the 1st discharge process mentioned above. The 1st irreversible capacity was observed because the electronic structures of sulfur in $a\text{-MoS}_3$ after the 1st charge were not similar to those before cycling. The electronic structures of sulfur after the 10th charge were similar to those after the 1st charge. Thus, the all-solid-state cell with $a\text{-MoS}_3$ showed relatively good cyclability after the 1st cycle.

The differences of the obtained capacity are discussed from the viewpoint of density of states (DOS) of $a\text{-TiS}_3$ and $a\text{-MoS}_3$. The cell with $a\text{-TiS}_3$ showed the reversible capacity of about 510 mAh g^{-1} for 10 cycles. This capacity was mainly attributable to the redox of sulfur during charge-discharge tests. On the other hand, the 1st charge capacity of the cell with $a\text{-MoS}_3$ was about 720 mAh g^{-1} and the irreversible capacity of 40 mAh g^{-1} was observed. The cell maintained the capacity of about 670 mAh g^{-1} up to the 10th cycle. Charge-discharge capacity of $a\text{-MoS}_3$ was based on the redox of both sulfur and molybdenum.

The DOS of $c\text{-TiS}_3$ and $a\text{-MoS}_3$ have been already reported [40, 41]. The S_{3p} electrons in $c\text{-TiS}_3$ are occupied near the Fermi level [40], indicating that the redox of sulfur mainly occurs for $c\text{-TiS}_3$. In this study, $a\text{-TiS}_3$ was prepared from $c\text{-TiS}_3$. In addition, the valence band XPS spectrum (in the range 0–50 eV) of $a\text{-TiS}_3$ was comparable to that of $c\text{-TiS}_3$ (data are not shown) and we thus believe that the DOS of $a\text{-TiS}_3$ is similar to that of $c\text{-TiS}_3$. As the result, the redox of sulfur mainly takes place for $a\text{-TiS}_3$. On the other hand, the S_{3p} and Mo_{4s} electrons are occupied near the Fermi level in $a\text{-MoS}_3$ [41]. Therefore, the redox of both sulfur and molybdenum occurs. The electrochemical redox species considered from XPS and XANES results agree with those from DOS of $a\text{-TiS}_3$ and $a\text{-MoS}_3$. Electronic structure changes of $a\text{-TiS}_3$ and $a\text{-MoS}_3$ in the cells with a conventional organic liquid electrolyte have not been reported, but we believe they are similar to those studied here in the all-solid-state cells. The 1st irreversible capacity of the cell using $a\text{-MoS}_3$ was observed. The cut-off voltage of all-solid-state cell with $a\text{-MoS}_3$ was lower than that of $a\text{-TiS}_3$ and the difference of cut-off voltage is a possible reason for the irreversible capacity in $a\text{-MoS}_3$. The electrochemical test for the cell with $a\text{-MoS}_3$ has thus been demonstrated at the same cut-off

of 0.5 V as the cell with *a*-TiS₃.

Figure 8 shows (a) the 1st charge-discharge curves of all-solid-state cell with *a*-MoS₃ at the cut-off voltage of 0.5 V vs. Li-In and (b) the S_{2p} XPS spectra of *a*-MoS₃ after the 1st charge. The cell with *a*-MoS₃ showed the discharge capacity of about 550 mAh g⁻¹, which was similar to the capacity of the cell with *a*-TiS₃. However, the cell with *a*-MoS₃ showed an 1st irreversible capacity of 60 mAh g⁻¹. The S_{2p} XPS spectrum of *a*-MoS₃ after the 1st charge mainly showed the two S_{2p_{3/2}} peaks at 159.9 and 161.4 eV. These two S_{2p_{3/2}} peaks were the same position as that after the 1st full discharge (cut-off of 0 V) (Fig. 5 (b)). It was found that the irreversible structure changes of *a*-MoS₃ occurred even though the cut-off voltage of the cell with *a*-MoS₃ was the same as that with *a*-TiS₃.

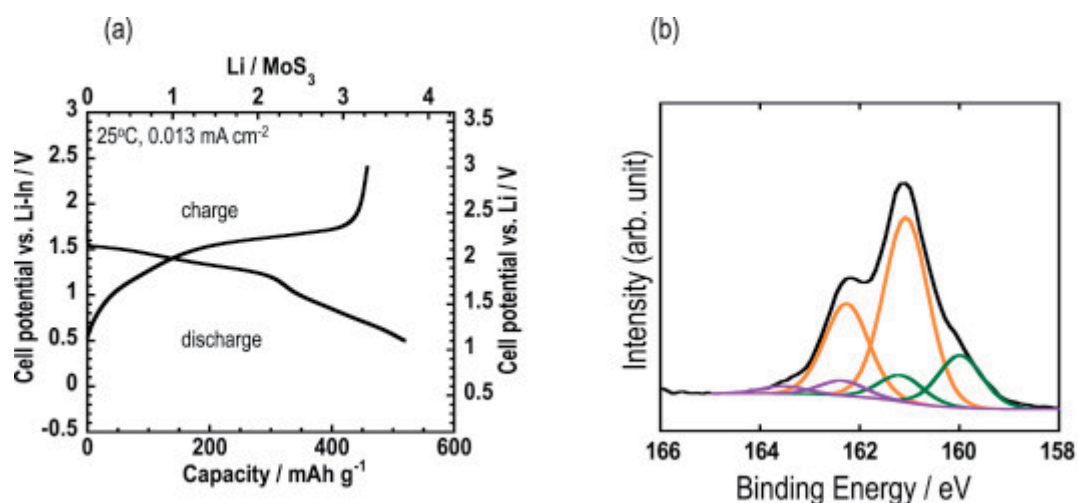


Fig. 8. (a) The 1st charge-discharge curve of all-solid-state cell with *a*-MoS₃ at the cut-off voltage of 0.5 V and (b) the S_{2p} XPS spectra of *a*-MoS₃ after the 1st charge.

Finally, the difference of the 1st reversibility of *a*-TiS₃ and *a*-MoS₃ is discussed. The electrode of *a*-TiS₃ was composed of S²⁻ and S₂²⁻ species and the electronic structures of sulfurs were similar to those in *c*-TiS₃. The electronic structures of these sulfur species changed reversibly during the 1st charge-discharge tests and thus the coulombic efficiency of the cell with *a*-TiS₃ was almost 100%. The reversible changes of sulfur electronic structures in *a*-TiS₃ were observed up to the 10th cycle and this brought about good cyclability of *a*-TiS₃. On the other hand, the electronic structures of sulfurs in *a*-MoS₃ were S²⁻ and S^{δ-}. The S_{2p} XPS spectrum was shifted to the lower binding energy side after the 1st full discharge. The peak positions of two S_{2p_{3/2}} peaks after the 1st charge were different from those before tests and almost the same as those after the 1st full discharge. As a result, the 1st reversibility of the cell with *a*-MoS₃ was inferior compared to that with *a*-TiS₃. Because the S_{2p} XPS and S *K*-edge XANES profiles after the 10th charge were similar to those after the 1st full discharge, the electronic structures of sulfur after the 10th charge were similar to

those after the 1st charge. Therefore, the cell showed good cyclability up to the 10th cycle. As described above, *a*-TiS₃ showed a superior initial reversibility. Sulfurs (S²⁻ and S₂²⁻) and titanium atoms in *a*-TiS₃ have chemical bonding similar to that in *c*-TiS₃ and strong interactions between the sulfurs and titanium would retain during the 1st cycle. On the other hand, S^{δ-} in *a*-MoS₃ may have weaker interactions to molybdenum atoms than S²⁻ in MoS₂ nano-clusters. One of the reason is the fact that *a*-MoS₃ was prepared by milling of crystalline sulfur and molybdenum metal. The difference in sulfur electronic structures is a possible reason for the 1st irreversible capacity in *a*-MoS₃. Sulfurs species lithiated at the 1st discharge process have similar electronic structures as sulfurs after the 1st and 10th charge, and thus sulfurs formed at the 1st discharge would have strong interactions to molybdenum atoms. In order to design the sulfur-rich transition metal sulfide electrodes with high capacity as well as good cyclability, sufficient interactions between sulfur and transition metal in the electrodes is important.

4. Conclusions

We have firstly examined the electronic structure changes of amorphous TiS₃ and MoS₃ electrodes in all-solid-state lithium batteries during cycling. In the case of *a*-TiS₃, the all-solid-state cell with *a*-TiS₃ maintained the reversible capacity of about 510 mAh g⁻¹ for the 10th cycles. The reversible sulfur redox of both S²⁻ and S₂²⁻ in *a*-TiS₃ mainly occurred during charge-discharge process. On the other hand, the 1st discharge and charge capacities of the cell with *a*-MoS₃ were about 760 and 720 mAh g⁻¹, respectively. The S_{2p} XPS and S *K*-edge XANES profiles after the 1st and 10th charge process were similar to those after the 1st discharge and were different from those before charge-discharge measurements. The irreversible sulfur redox of both S²⁻ and S^{δ-} in *a*-MoS₃ was observed, while the reversible electronic structure changes of molybdenum were observed at the 1st cycle. The all-solid-state cell with *a*-MoS₃ showed relatively good cyclability except for the 1st cycle. Electrochemical performance of the cells using *a*-MS₃ (M: Ti and Mo) was affected by electronic structures of sulfurs in *a*-MS₃.

Acknowledgement

This research was financially supported by the Japan Science and Technology Agency, Advanced Low Carbon Technology Research and Development Program (ALCA), Specially Promoted Research for Innovative Next Generation Batteries (SPRING) Project.

References

- [1] T. Matsuyama, M. Deguchi, K. Mitsuhara, T. Ohta, T. Mori, Y. Orikasa, Y. Uchimoto, Y. Kowada, A. Hayashi, M. Tatsumisago, *J. Power Sources*, **313**, 104 (2016).
- [2] J.M. Tarascon, M. Armand, *Nature*, **414**, 359 (2001).
- [3] A.S. Arico, P. Bruce, B. Scrosati, J.M. Tarascon, W. Van Schalkwijk, *Nature Mater.*, **4**, 366 (2005).
- [4] R. Komiya, A. Hayashi, H. Morimoto, M. Tatsumisago, T. Minami, *Solid State Ionics*, **140**, 83 (2001).
- [5] F. Mizuno, S. Hama, A. Hayashi, K. Tadanaga, T. Minami, M. Tatsumisago, *Chem. Lett.*, **31**, 1244 (2002).
- [6] F. Mizuno, A. Hayashi, K. Tadanaga, M. Tatsumisago, *J. Power Sources*, **146**, 711 (2005).
- [7] M. Tatsumisago, A. Hayashi, *Funct. Mater. Lett.*, **1**, 31 (2008).
- [8] A. Pradel, M. Ribes, *Solid State Ionics*, **18**, 351 (1986).
- [9] F. Mizuno, A. Hayashi, K. Tadanaga, M. Tatsumisago, *Adv. Mater.*, **17**, 918 (2005).
- [10] R. Mercier, J.P. Malugani, B. Fahys, G. Robert, *Solid State Ionics*, **5**, 663 (1981).
- [11] N. Kamaya, K. Homma, Y. Yamakawa, M. Hirayama, R. Kanno, M. Yonemura, T. Kamiyama, Y. Kato, S. Hama, K. Kawamoto, A. Mitsui, *Nature Mater.*, **10**, 682 (2011).
- [12] Y. Seino, T. Ota, K. Takada, A. Hayashi, M. Tatsumisago, *Energy Environ. Sci.*, **7**, 627 (2014).
- [13] G.L. Holleck, J.R. Driscoll, *Electrochim. Acta*, **22**, 647 (1977).
- [14] Y. Onuki, R. Inada, S. Tanuma, S. Yamanaka, H. Kamimura, *Solid State Ionics*, **11**, 195 (1983).
- [15] M.H. Lindic, H. Martinez, A. Benayad, B. Pecquenard, P. Vinatier, A. Levasseur, D. Gonbeau, *Solid State Ionics*, **176**, 1529 (2005).
- [16] A. Hayashi, T. Matsuyama, A. Sakuda, M. Tatsumisago, *Chem. Lett.*, **41**, 886 (2012).
- [17] T. Matsuyama, A. Hayashi, T. Ozaki, S. Mori, M. Tatsumisago, *J. Mater. Chem. A*, **3**, 14142 (2015).
- [18] A. Sakuda, N. Taguchi, T. Takeuchi, H. Kobayashi, H. Sakaebe, K. Tatsumi, Z. Ogumi, *Electrochem. Commun.*, **31**, 71 (2013).
- [19] A. Sakuda, N. Taguchi, T. Takeuchi, H. Kobayashi, H. Sakaebe, K. Tatsumi, Z. Ogumi, *Solid State Ionics*, **262**, 143 (2014).
- [20] A. Sakuda, N. Taguchi, T. Takeuchi, H. Kobayashi, H. Sakaebe, K. Tatsumi, Z. Ogumi, *ECS Electrochem. Lett.*, **3**, A79 (2014).
- [21] T. Matsuyama, A. Sakuda, A. Hayashi, Y. Togawa, S. Mori, M. Tatsumisago, *J. Solid*

- State Electrochem.*, **17**, 2697 (2013).
- [22] T. Matsuyama, A. Hayashi, T. Ozaki, S. Mori, M. Tatsumisago, *J. Ceram. Soc. Jpn.*, **124**, 242 (2016).
- [23] T. Matsuyama, M. Deguchi, A. Hayashi, M. Tatsumisago, T. Ozaki, Y. Togawa, S. Mori, *Electrochemistry*, **83**, 889 (2015).
- [24] Y. Diao, K. Xie, S. Xiong, X. Hong, *J. Electrochem. Soc.*, **159**, A1816 (2012).
- [25] J. Song, S.J. Lee, Y. Kim, S.-S. Kim, K.T. Lee, N.-S. Choi, *ECS Electrochem. Lett.*, **3**, A26 (2014).
- [26] X. Liang, C. Hart, Q. Pang, A. Garsuch, T. Weiss, L.F. Nazar, *Nature Comm.*, **6**, 5682 (2015).
- [27] J. Yan, X. Liu, H. Qi, W. Li, Y. Zhou, M. Yao, B. Li, *Chem. Mater.*, **27**, 6394 (2015).
- [28] M. Helen, M.A. Reddy, T. Diemant, U. Golla-Schindler, R.J. Behm, U. Kaiser, M. Fichtner, *Sci. Rep.*, **5**, 12146 (2015).
- [29] J. Gao, M.A. Lowe, Y. Kiya, H.D. Abruna, *J. Phys. Chem. C*, **115**, 25132 (2011).
- [30] M. Cuisinier, P.-E. Cabelguen, S. Evers, G. He, M. Kolbeck, A. Garsuch, T. Bolin, M. Balasubramanian, L.F. Nazar, *J. Phys. Chem. Lett.*, **4**, 3227 (2013).
- [31] M. Cuisinier, P.E. Cabelguen, B.D. Adams, A. Garsuch, M. Balasubramanian, L.F. Nazar, *Energy Environ. Sci.*, **7**, 2697 (2014).
- [32] M.A. Lowe, J. Gao, H.D. Abruna, *Rsc Advances*, **4**, 18347 (2014).
- [33] Q. Pang, D. Kundu, M. Cuisinier, L.F. Nazar, *Nature Comm.*, **5**, 4759 (2014).
- [34] M. Cuisinier, C. Hart, M. Balasubramanian, A. Garsuch, L.F. Nazar, *Adv. Energy Mater.*, **5**, 1401801 (2015).
- [35] Y. Gorlin, A. Siebel, M. Piana, T. Huthwelker, H. Jha, G. Monsch, F. Kraus, H.A. Gasteiger, M. Tromp, *J. Electrochem. Soc.*, **162**, A1146 (2015).
- [36] R. Dominko, M.U.M. Patel, V. Lapornik, A. Vizintin, M. Kozelj, N.N. Tusar, I. Arcon, L. Stievano, G. Aquilanti, *J. Phys. Chem. C*, **119**, 19001 (2015).
- [37] M.E. Fleet, S.L. Harmer, X. Liu, H.W. Nesbitt, *Surf. Sci.*, **584**, 133 (2005).
- [38] A. Hayashi, S. Hama, T. Minami, M. Tatsumisago, *Electrochem. Commun.*, **5**, 111 (2003).
- [39] Z. Zeng, Z. Yin, X. Huang, H. Li, Q. He, G. Lu, F. Boey, H. Zhang, *Angew. Chem. Int. Ed.*, **50**, 11093 (2011).
- [40] M. Abdulsalam, D.P. Joubert, *Eur. Phys. J. B*, **88**, (2015).
- [41] G.F. Khudorozhko, I.P. Asanov, L.N. Mazalov, E.A. Kravtsova, G.K. Parygina, V.E. Fedorov, Y.V. Mironov, *J. Struct. Chem.*, **35**, 823 (1994).